GEOPHYSICAL RESEARCH LETTERS, VOL. 30, NO. 17, 1907, doi:10.1029/2003GL017676, 2003

Semi-diurnal and diurnal tidal dissipation from TOPEX/Poseidon altimetry

Gary D. Egbert
College of Oceanic and Atmospheric Sciences, Oregon State University, Corvallis, Oregon, USA

Richard D. Ray
NASA Goddard Space Flight Center, Greenbelt, Maryland, USA

Received 2 May 2003; accepted 29 July 2003; published 12 September 2003.

[1] Tidal energy dissipation is estimated for eight semi-diurnal and diurnal constituents using a global inverse solution constrained by TOPEX/Poseidon altimeter data. Very similar spatial patterns are obtained for all semi-diurnal constituents, with about one third of the total dissipation occurring in the deep ocean over rough topography. Maps for diurnal constituents are also similar amongst themselves, but quite different from the semi-diurnal results. For diurnals a smaller fraction of dissipation, roughly 10%, occurs in the deep ocean. Much of the difference can be explained by the very different spatial pattern of diurnal and semi-diurnal tidal currents. The lack of free internal waves at frequencies poleward of 30° at diurnal frequencies also probably plays a role, limiting the effectiveness of baroclinic conversion as an energy sink for barotropic diurnal tides. *INDEX TERMS:* 4560 Oceanography: Physical: Surface waves and tides (1255); 1255 Geodesy and Gravity: Tides—ocean (4560); 4544 Oceanography: Physical: Internal and inertial waves. **Citation:** Egbert, G. D., and R. D. Ray, Semi-diurnal and diurnal tidal dissipation from TOPEX/Poseidon altimetry, *Geophys. Res. Lett.*, *30*(17), 1907, doi:10.1029/2003GL017676, 2003.

1. Introduction

[2] *Egbert and Ray* [2001; see also *Egbert and Ray*, 2000] presented empirical maps of tidal dissipation in the global ocean based on TOPEX/Poseidon (T/P) altimeter data, demonstrating that a significant fraction (25–35%) of barotropic tidal energy is lost in the deep ocean over rough topography. Although the T/P data only directly constrain the spatial pattern of open ocean dissipation, this pattern, and other evidence [*Ray and Mitchum*, 1997; *Egbert and Ray*, 2001] support the inference that energy losses from the surface tides in the deep ocean must result from conversion into internal tides. The analysis of *Egbert and Ray* [2001] was restricted to the dominant semi-diurnal M_2 constituent, which accounts for roughly 2/3 of all tidal dissipation. In this paper we present estimates of dissipation computed for seven additional tidal constituents, both semi-diurnal and diurnal. The largest of these dissipate almost an order of magnitude less energy than M_2, so we can anticipate significantly greater difficulties with noise.

0094-8276/03/2003GL017676$05.00

[3] As in *Egbert and Ray* [2001] the dissipation rate is estimated as the balance between work done by tidal forces and the divergence of tidal energy flux

$$D = W - \nabla \cdot \mathbf{P} = \rho g \left\langle \mathbf{U} \cdot \nabla \left(\zeta_{EQ} + \zeta_{SAL} \right) \right\rangle - \rho g \nabla \cdot \langle \mathbf{U} \zeta \rangle. \quad (1)$$

Here ζ and $\mathbf{U}$ are tidal elevations and volume transports, ζ_{EQ} is the equilibrium tide, ζ_{SAL} accounts for ocean self-attraction and loading, and the brackets $\langle\ \rangle$ denote time averages. T/P directly constrains ζ, and from this ζ_{SAL} can be readily calculated [*Ray*, 1998]. *Egbert and Ray* [2001] estimated $\mathbf{U}$ by fitting altimetrically constrained elevations and the shallow water equations (SWE) with two different least squares (LS) procedures. In the first approach, the variational data assimilation scheme of *Egbert et al.* [1994] was used to estimate both ζ and $\mathbf{U}$ by minimizing a weighted misfit to the T/P data and the SWE. In the second approach, gridded tidal elevation fields ζ estimated empirically from T/P altimeter data were substituted into the SWE, and the volume transports $\mathbf{U}$ were estimated by weighted LS, minimizing residuals in the dynamical equations. Provided mass conservation was strongly enforced, similar dissipation maps for M_2 were obtained with both approaches. For the additional constituents considered here dissipation maps obtained by the two approaches are similar for S_2 and K_1, but for the smaller constituents maps derived from the empirical solution are rather noisy. We thus focus on the generally cleaner results obtained with the variational assimilation approach.

2. Results

[4] Dissipation maps were computed for 8 tidal constituents (M_2, S_2, N_2, K_2, K_1, O_1, P_1, Q_1) using TPXO.5, an updated 1/2° nearly global (86°S–82°N) version of the global assimilation solution described in *Egbert et al.* [1994]. TPXO.5 assimilates T/P data from 232 orbit cycles low-pass filtered along-track and sampled at all crossovers, plus 4 points in between. Further details on the assimilation, including the dynamical equations and bathymetry, are given in *Egbert and Erofeeva* [2002] and *Egbert and Ray* [2001]. Dissipation estimates for four of the constituents are given in Figure 1. For the two semi-diurnal constituents plotted (M_2 and N_2) the range of the color scale has been set proportional to the square of the amplitude of the equilibrium tidal elevation (0.244 m for M_2 vs. 0.046 m for N_2, so the full range for N_2 is smaller by a factor of

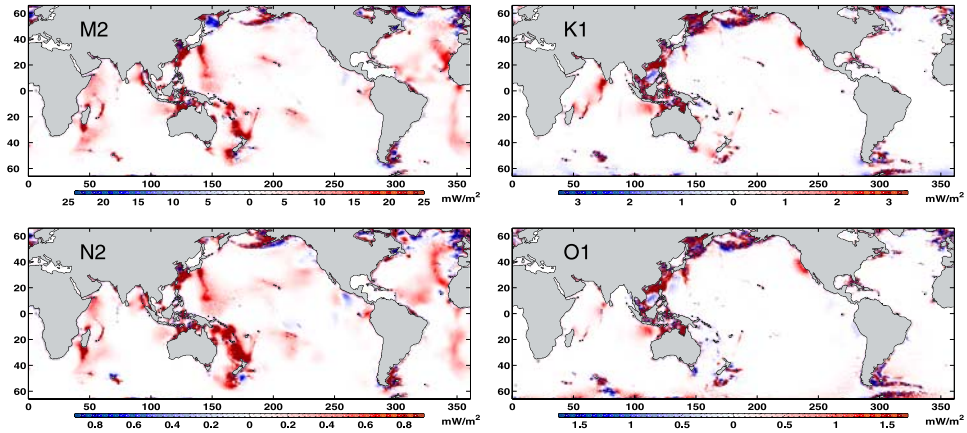

Figure 1. Dissipation maps for four constituents from the TPXO.5 global tidal solution. (a) M_2, (b) N_2, (c) K_1, (d) O_1.

$(0.046/0.244)^2$ = .036). With this scaling, the two semi-diurnal dissipation maps are very similar to each other, and to all of the T/P based M_2 maps presented previously in *Egbert and Ray* [2001]. Dissipation in the deep ocean is strongly enhanced over major topographic features, including the trenches and back-arcs in the Western Pacific, and the Mid-Atlantic and Western Indian Ridges. The Hawaiian Ridge and Tuamoto Archipelago (Tahiti) also show up clearly in maps for both constituents.

[5] Maps for S_2 and K_2 are also generally similar when plotting ranges are chosen proportional to the square of equilibrium amplitudes, and are not shown. The map for S_2 is the most anomalous of the four semi-diurnal constituents. This almost certainly reflects the fact that the S_2 ocean tide is forced in part by insolation induced atmospheric pressure variations [*Cartwright and Ray*, 1994], which have not been properly accounted for in either the prior model for TPXO.5, or in our calculations of the work term W in (1). A correct treatment of S_2 is further complicated by aliasing of this 12 hour tide in the 6-hour pressure fields used for the inverted barometer correction that has been applied to the T/P data before fitting the tidal model [*Ponte and Ray*, 2002].

[6] The total dissipation, and the division between deep and shallow seas is summarized in Table 1. The division between shallow and deep areas is as in *Egbert and Ray* [2001], with the boundary drawn well out into the deep ocean to avoid areas with bathymetric complications where errors in tidal current estimates are expected to be greatest. For M_2, N_2, and K_2 there is excellent agreement on the fraction of deep dissipation, at approximately 32%. S_2 is again the most anomalous of the semi-diurnal constituents (37% deep), almost certainly reflecting biases due to neglect of radiation forcing.

[7] The pattern of dissipation for the diurnal constituents is distinctly different. Maps for the two largest diurnal constituents (K_1 and O_1) are given in Figure 1c–1d, with relative scaling of these two constituents again proportional to the square of the equilibrium amplitude. Results for P_1 are qualitatively similar and are not shown. The maps for Q_1, which is by far the smallest constituent considered, are too noisy to be useful. For the diurnal constituents evidence for dissipation in the deep ocean is generally not so clear. In contrast to the semi-diurnal constituents, there is essentially no dissipation in the deep Atlantic, which is expected since all diurnal tides are very small throughout the Atlantic. Dissipation in the open ocean in the Western Pacific is also much reduced, and only in the Indian Ocean at low latitudes is there very clear evidence for dissipation in deep water over rough topography. There are hints of enhanced dissipation over the Hawaiian ridge and Tuamoto archipelago, but this is not so clear as in the semi-diurnal maps. For the diurnal constituents only about 10% of the dissipation occurs in the deep ocean (Table 1), a result which is consistent for all 4 diurnal constituents in TPXO.5.

[8] A rough indication of the level of errors in the deep ocean dissipation estimates is provided by comparison to results obtained from LS fitting of currents to the GOT99 [*Ray*, 1999] tidal solution. The global total dissipation depends only on the tidal elevation [e.g., *Egbert and Ray*, 2001] which is directly constrained by T/P. As a result, totals for TPXO.5 and GOT99 agree within a few GW for

Table 1. Total Dissipation, PE and KE, and Division Between Deep and Shallow Seas[a]

	Dissipation (TW)			TPXO.5	GOT99	($\times 10^{15}$ J)		
Tide	Total	Shallow	Deep	% Deep	% Deep	PE	KE	%KE Shallow
M_2	2.435	1.649	0.782	32.2	25.9	134.40	177.86	20
S_2	0.376	0.237	0.139	37.0	33.6	21.11	28.76	20
N_2	0.110	0.076	0.034	31.0	24.7	5.97	8.14	23
K_2	0.030	0.020	0.010	32.9	35.0	1.72	2.34	21
K_1	0.343	0.304	0.039	11.3	16.9	18.51	31.41	39
O_1	0.173	0.153	0.021	11.8	11.2	8.84	16.03	37
P_1	0.035	0.032	0.003	9.6		1.77	3.01	36
Q_1	0.007	0.006	0.001	13.2		0.41	0.75	38
Total	3.508	2.477	1.028	29.3		192.73	268.30	

[a]Shallow/deep division (as defined in *Egbert and Ray* [2001]) is given for the TPXO.5 assimilation solution, and for GOT99.

all constituents except S_2, for which the radiation forcing (which is treated more properly in GOT99) is again a complicating factor. There are significantly greater differences in the division between shallow and deep areas, which is given for both TPXO.5 and GOT99 in Table 1 for all constituents except P_1 (which is obtained from K_1 by inference in GOT99 and is thus not independent), and for Q_1 which is too small to produce sensible results with the empirical approach. Differences between the TPXO.5 and GOT99 results suggest error bars of roughly 20% for the deep water totals, perhaps somewhat greater for the diurnals.

[9] Much of the dissipation for the diurnal constituents is concentrated in a few marginal seas around the northern and western Pacific basin. This is quite different from the much more uniform distribution of dissipation around the globe seen for the semi-diurnal constituents [cf. *Egbert and Ray*, 2001, their Plate 3]. The Okhotsk and China Seas each account for over 15% of the global total dissipation for all diurnal constituents, while the Bering Sea accounts for roughly 10%. Together almost half of the diurnal constituent dissipation occurs in these three marginal seas. Other significant diurnal sinks include the Northwest Australian shelf (about 7%) and Antarctica (about 15%). Note that while the spatial distribution of dissipation around Antarctica is not constrained by the T/P data (which does not extend south of 66°S), the total dissipation in this area can be accurately estimated. As in *Ray and Egbert* [1997] the total flux of energy toward Antarctica can be estimated from the altimeter data. Furthermore, comparison to tide gauges shows that the K_1 elevations in TPXO.5 are accurate to within 4 cm RMS around Antarctica (S. Y. Erofeeva, personal communication), so the integrated local work term W (which is non-negligible for diurnals, but only requires elevations; see *Egbert and Ray* [2001]) is also estimated with reasonable accuracy.

[10] Other features of note (which are also clear in the GOT99 dissipation maps) are the enhancement of dissipation in both the K_1 and O_1 maps off the west coast of North America and around the the entrance to the Gulf of Mexico, and the areas of negative dissipation at the bottom of the K_1 (but not the O_1) map. This last feature is certainly an artifact, possibly the result of inaccuracies in the K_1 elevations, which are aliased with ocean signals of semi-annual period by the T/P sampling, particularly at high latitudes [*Andersen and Knudsen*, 1997]. The enhancement of dissipation off the west coast of North America may also be an artifact. It is unclear why dissipation should be enhanced in these patches centered at about 35°, but not further north where generally larger diurnal amplitudes and stronger shelf currents associated with topographic vorticity waves might be expected to lead to greater dissipation [*Foreman et al.*, 2000].

3. Discussion

[11] For TPXO.5 tidal constituents were fitted to the altimeter data independently. Individual constituents are linked only indirectly through the quadratic drag law used for the time-stepped prior solution, and for the linearized drag coefficient used in the assimilation. The quadratic drag law leads to essentially no deep ocean dissipation in the prior. Furthermore, *Egbert and Ray* [2001] show that dissipation maps obtained from assimilation solutions are insensitive to a priori assumptions about drag coefficients, so the similarity between dissipation estimates for different semi-diurnal constituents cannot be attributed reasonably to this weak coupling. The results of Figure 1 and Table 1 thus offer further support for the conclusions of *Egbert and Ray* [2001] that roughly a third of all tidal energy dissipation occurs in the deep ocean over areas of rough topography. *Egbert and Ray* [2000] suggested a rough extrapolation of the M_2 results to 1 TW of deep ocean dissipation for all constituents. This rough estimate is confirmed explicitly here (Table 1). Our results show that dissipation for constituents of a fixed species (diurnal or semi-diurnal) scales with the square of equilibrium amplitude (Table 1). This implies that a linearized drag law can account for dissipation quite well, at least in a global sense. This conclusion is consistent with the usual parameterizations of tidal dissipation, since the quadratic law for bottom drag in shallow seas can be accurately linearized around a dominant constituent (M_2 or in some places K_1; see *Le Provost and Poncet* [1978]), and energy dissipation due to barotropic/baroclinic conversion can be parameterized with a linear drag law [e.g., *Sjöberg and Stigebrandt*, 1992; *Jayne and St. Laurent*, 2001].

[12] The significant differences between dissipation maps for diurnal and semi-diurnal constituents can be explained mostly by differences in the patterns of barotropic tidal currents. The total kinetic (KE) and potential (PE) energy for all TPXO.5 constituents is given in Table 1, along with the division of KE between deep and shallow water. For the diurnal constituents almost 40% of the total KE is localized in shallow seas, while for semi-diurnal constituents this fraction is just over 20%. Given that diurnal motions are more heavily concentrated in shallow seas, it is not surprising that bottom drag plays a relatively larger role in dissipation for these constituents.

[13] Differences in the spatial distribution of tidal kinetic energy, plotted for M_2 and K_1 in Figure 2, explain some further aspects of the dissipation maps. To emphasize differences in spatial distributions a logarithmic scale is used in Figure 2, with the plotting range scaled by the total kinetic energy in deep water. Thus, for both constituents areas of the same color correspond to similar relative fractions of deep ocean kinetic energy. Diurnal currents throughout most of the Atlantic are very small, so baroclinic conversion would be expected to be weak over the mid-Atlantic ridge. This is consistent with the absence of significant dissipation in the deep Atlantic for diurnal constituents. There are significant diurnal currents in the equatorial Indian Ocean, just where we find evidence for deep ocean dissipation of diurnal tides. The shift of the most prominent area of Indian Ocean dissipation from the West Indian ridge (south of Madagascar) to the mid-Indian ridge system southwest of the sub-continent is also consistent with differences in the patterns of diurnal and semi-diurnal tidal currents in this basin. Not surprisingly, the highest diurnal kinetic energies occur around the North Pacific rim where dissipation for the diurnal constituents is concentrated.

[14] Thus, much of the difference between semi-diurnal and diurnal dissipation patterns can be explained by differ-

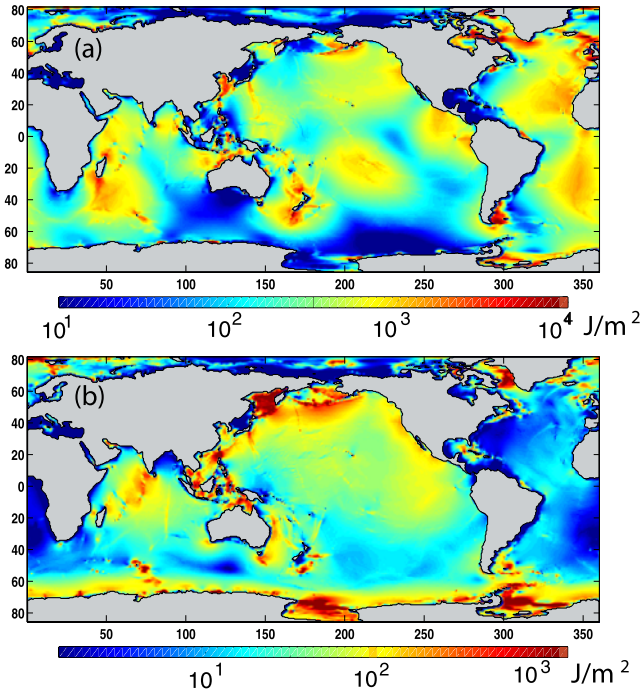

Figure 2. Vertically integrated kinetic energy for (a) M_2 and (b) K_1. The color scale is logarithmic with the range scaled by the total kinetic energy in deep water.

ences in the spatial distribution of barotropic tidal currents. However, for diurnal and semi-diurnal constituents with comparable levels of deep-ocean kinetic energy (e.g., K_1 and S_2; O_1 and N_2) deep ocean dissipation rates are always substantially greater for the semi-diurnals, suggesting that the dependence of barotropic/baroclinic conversion on frequency probably also plays a role. Poleward of the critical latitude where $\omega < f$ (roughly 30 degrees for diurnals, but only near the pole for semi-diurnals) there are no free internal waves over a flat bottom. In this sub-inertial regime baroclinic disturbances generated by flow over topography would remain trapped to the topography. Linear inviscid theories for generation of internal tides over weak topography [e.g., *Bell*, 1975; *Llewellyn Smith and Young*, 2001] predict that averaged over a tidal cycle there would be no net barotropic/baroclinic energy conversion at sub-inertial frequencies.

[15] With stronger topographic variations and dissipation the situation is less clear-cut. Baroclinic disturbances could propagate away from generation sites along ridges, volcanic arcs or coasts. Locally trapped baroclinic waves may also lose significant energy to turbulence and mixing, thus effectively extracting energy from the surface tides in the sub-inertial regime. Dissipation maps for the diurnal constituents are at least consistent with this picture. Only at subcritical latitudes (mostly in the Indian Ocean) is there any evidence for significant open ocean barotropic dissipation.

[16] At higher latitudes all significant areas of diurnal dissipation occur along the edges of basins. Some of this dissipation (e.g., along the Aleutian arc, east of New Zealand and possibly even along the west coast of North America), could involve enhanced dissipation associated with small scale shelf or other topographically trapped waves modified by stratification. Since the momentum equations are treated as weak constraints for mapping dissipation, the energetic effects on the large scale surface tide of such small scale (generally baroclinic) processes can in principal be revealed even if the processes themselves are not resolved or properly parameterized; see *Egbert and Ray* [2001] for extensive discussion. However, with the coarse resolution of the global dissipation maps it is not possible to clearly separate dissipation that may be associated with vorticity waves along shelf edges from the bottom drag expected in adjacent shallow seas. More detailed local studies using data from multiple satellites may allow such resolution in the future.

[17] **Acknowledgments.** This work was supported by the National Aeronautics and Space Administration, and by National Science Foundation grant OCE-9819518 to GDE.

References

Andersen, O. B., and P. Knudsen, Multi-satellite ocean tide modeling—the K_1 constituent, *Progr. Oceanogr.*, *40*, 197–216, 1997.

Bell, T. H., Topographically generated internal waves in the open ocean, *J. Geophys. Res.*, *80*, 320–327, 1975.

Cartwright, D. E., and R. D. Ray, On the radiational anomaly in the global ocean tide, with reference to satellite altimetry, *Oceanolog. Acta*, *17*, 453–459, 1994.

Egbert, G. D., and R. D. Ray, Significant tidal dissipation in the deep ocean inferred from satellite altimeter data, *Nature*, *405*, 775–778, 2000.

Egbert, G. D., and R. D. Ray, Estimates of M2 Tidal Energy Dissipation from TOPEX/Poseidon Altimeter Data, *J. Geophys. Res.*, *106*, 22,475–22,502, 2001.

Egbert, G. D., and S. Y. Erofeeva, Efficient inverse modeling of barotropic ocean tides, *J. Atmos. Ocean. Tech.*, *19*, 183–204, 2002.

Egbert, G. D., A. F. Bennett, and M. G. G. Foreman, Topex/Poseidon tides estimated using a global inverse model, *J. Geophys. Res.*, *99*, 24,821–24,852, 1994.

Foreman, M. G. G., W. R. Crawford, J. Y. Cherniawsky, R. F. Henry, and M. R. Tarbotton, A high-resolution assimilating tidal model for the northeast Pacific Ocean, *J. Geophys. Res.*, *105*, 28,629–28,651, 2000.

Jayne, S. R., and L. C. St. Laurent, Parameterizing tidal dissipation over rough topography, *Geophys. Res. Lett.*, *28*, 811–814, 2001.

Le Provost, C., and A. Poncet, Finite element method for spectral modeling of tides, *Int. J. Numer. Methods Eng.*, *12*, 853–871, 1978.

Llewellyn Smith, S. G., and W. R. Young, Conversion of the barotropic tide, *J. Phys. Ocean.*, *32*, 1554–1566, 2001.

Ponte, R. M., and R. D. Ray, Atmospheric pressure corrections in geodesy and oceanography: A strategy for handling air tides, *Geophys. Res. Lett.*, *29*(24), 2153, 2002.

Ray, R. D., Ocean self-attraction and loading in numerical tidal models, *Marine Geodesy*, *21*, 181–192, 1998.

Ray, R. D., A global ocean tide model from TOPEX/Poseidon altimetry, GOT99. 2, NASA Tech. Memo. 209478, 1999.

Ray, R. D., and G. D. Egbert, The flux of tidal energy across latitude 60S, *Geophys. Res. Lett.*, *24*, 543–546, 1997.

Ray, R. D., and G. T. Mitchum, Surface manifestation of internal tides in the deep ocean: Observations from altimetry and island gauges, *Progr. Oceanogr.*, *40*, 135–162, 1997.

Sjöberg, B., and A. Stigebrandt, Computations of the geographical distribution of the energy flux to mixing processes via internal tides and the associated vertical circulation in the ocean, *Deep Sea Res.*, *39*, 269–291, 1992.

G. D. Egbert, College of Oceanic and Atmospheric Sciences, Ocean. Admin. Bldg. 104, Oregon State University, Corvallis, OR 97331-5503, USA. (egbert@oce.orst.edu)

R. D. Ray, NASA Goddard Space Flight Center, Code 926, Greenbelt, MD 20771, USA. (richard.ray@gsfc.nasa.gov)